Electronic Paramagnetic Resonance and Magnetic Properties of Model Complexes for Binuclear Active Sites in Hydrolase Enzymes

Brian E. Schultz,[†] Bao-Hui Ye,[‡] Xiao-yuan Li,[‡] and Sunney I. Chan*[,†]

Arthur Amos Noyes Laboratory of Chemical Physics, California Institute of Technology, Pasadena, California 91125, and Department of Chemistry, The Hong Kong University of Science and Technology, Clear Water Bay, Kowloon, Hong Kong

Received August 14, 1996[⊗]

A set of binuclear metal complexes with the formula $M_2(Im)_4(OAc)_4(H_2O)$, where M = Mn, Co, or Ni, designed as mimics of the active sites of hydrolase enzymes, were subjected to EPR and magnetic susceptibility studies. The manganese complex displayed a broad EPR spectrum over the field range 0−5500 G. The 4 K spectrum was simulated as a summation of the $S = 1$, $S = 2$, and $S = 3$ spin manifolds of the coupled dimer, with each manifold weighted by the appropriate Boltzmann factor. Parameters for the best fits of EPR and magnetic susceptibility were $g = 1.95$, $J = -1.29$ cm^{-1}, and $D = 0.095$ cm^{-1}, with line widths of 350, 450, and 550 G for the $S = 1$, 2, and 3 manifolds, respectively. An alternative simulation, with $g = 1.93$, $J = -1.28$ cm^{-1}, and $D = 0.081$ cm^{-1} provided a better fit for the central peaks but only accounted for six of the seven observed peaks. The cobalt and nickel complexes are EPR-silent. Magnetic susceptibility measurements of these two dimers showed weak antiferromagnetic coupling; variable-temperature magnetic susceptibility plots were fit with the parameters $g = 2.22$, $J = -1.60$ cm^{-1} (cobalt) and $g = 2.04$, $J = -2.47$ cm^{-1} (nickel). The weak coupling highlights the difficulty in detecting bound water in these binuclear complexes or in enzymes and hence in determining active site structure through the physical techniques used in this work.

Introduction

Of the various enzymes utilized in biological systems to catalyze hydrolysis reactions, a significant number contain binuclear metal centers at their active sites, or possess three or more metal centers at the active site, yet maintain a binuclear motif as part of the active site structure. Several of these enzymes have been isolated and crystallographically characterized.[1−10] Metals utilized in these enzymes include magnesium, manganese, iron, cobalt, nickel, and zinc. For many of these proteins, the apoenzyme can be reconstituted with divalent metals other than those occurring naturally, with recovery of a substantial amount of activity. While the metal coordination environments vary markedly between enzymes, those binuclear metalloenzymes whose structures have been determined typically possess as common features aspartate or glutamate residues as bridging ligands, with terminal histidine and carboxylate ligation and metal-bound hydroxo or aquo groups occurring frequently.

The diversity of active site structures and metals utilized in the hydrolase enzymes raises questions concerning the mode of binding and activation of substrate molecules and the selection of metals for the various hydrolytic processes. For example, water molecules have been observed in both terminal and bridging binding modes in hydrolase enzymes, yet it is not clear which binding mode leads to water activation or whether the activation differs between enzymes. As part of an ongoing study to understand the role of the binuclear metal centers in the overall activity of the hydrolase enzymes, and to elucidate the overall mechanism of the hydrolysis reaction, a series of model complexes with the formula $M_2(Im)_4(OAc)_4(H_2O)$ were synthesized. The synthesis, structures, and optical properties of these compounds are presented elsewhere.[11] This paper presents a study of the electronic structure of these compounds as deduced from electron paramagnetic resonance spectroscopy and magnetic susceptibility measurements.

Experimental Section

The synthesis of the compounds $Mn_2(Im)_4(OAc)_4(H_2O)$, $Co_2(Im)_4(OAc)_4(H_2O)$, and $Ni_2(Im)_4(OAc)_4(H_2O)$ is given elsewhere.[11] EPR spectra were recorded on a Varian E-109 EPR spectrometer equipped with a Varian E-231 TE 102 rectangular cavity and interfaced to an IBM-compatible PC computer for data acquisition and analysis. Variable-temperature experiments utilized an Oxford Instruments ESR-900 liquid helium cryostat. Magnetic susceptibility measurements were made on a Quantum Design MPMS SQUID magnetometer. EPR spectra were simulated using spin Hamiltonian matrix diagonalization, with the program EPR-NMR (Department of Chemistry, University of Saskatchewan, Canada).

Results

The compounds $Mn_2(Im)_4(OAc)_4(H_2O)$, $Co_2(Im)_4(OAc)_4(H_2O)$, and $Ni_2(Im)_4(OAc)_4(H_2O)$ possess the structure shown

[†] California Institute of Technology.
[‡] The Hong Kong University of Science and Technology.
[⊗] Abstract published in *Advance ACS Abstracts,* May 15, 1997.

(1) Hough, E.; Hansen, L. K.; Birknes, B.; Jynge, K.; Hansen, S.; Hordvik, A.; Little, C.; Dodson, E.; Derewenda, Z. *Nature* **1989**, *338*, 357−360.
(2) Beese, L. S.; Steitz, T. A. *EMBO J.* **1991**, *10*, 25−33.
(3) Davies, J. F., II; Hostomska, Z.; Hostomsky, Z.; Jordan, S. R.; Matthews, D. A. *Science* **1991**, *252*, 88−95.
(4) Kim, E. E.; Wyckoff, H. W. *J. Mol. Biol.* **1991**, *218*, 449−464.
(5) Volbeda, A.; Lahm, A.; Sakiyama, F.; Suck, D. *EMBO J.* **1991**, *10*, 1607−1618.
(6) Roderick, S. L.; Matthews, B. W. *Biochemistry* **1993**, *32*, 3907−3912.
(7) Kim, H.; Lipscomb, W. N. *Biochemistry* **1993**, *32*, 8465−8478.
(8) Jabri, E.; Carr, M. B.; Hausinger, R. P.; Karplus, P. A. *Science* **1995**, *268*, 998−1004.
(9) Sträter, N.; Klabunde, T.; Tucker, P.; Witzel, H.; Krebs, B. *Science* **1995**, *268*, 1489−1492.
(10) Kanyo, Z. F.; Scolnick, L. R.; Ash, D. E.; Christianson, D. W. *Nature* **1996**, *383*, 554−557.
(11) Ye, B.-H.; Williams, I. D.; Li, X.-Y., manuscript in preparation.

S0020-1669(96)00988-3 CCC: $14.00

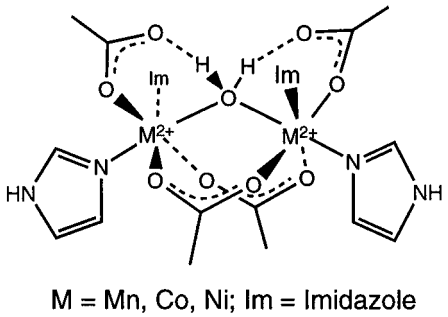

Figure 1. Schematic diagram of the bimetallic compounds studied in this work.

in Figure 1. Complete structural details are presented elsewhere.[11] They have a μ-aquo−bis(μ-carboxylato) bimetal core, with four terminal imidazole ligands and two terminal carboxylates. The terminal carboxylates form hydrogen-bonding interactions with the bridging aquo ligand, as is observed for other dimeric compounds with μ-aquo groups. In all of the dimers, a C_2 axis passes through the water bridge. The aquo group is labile, as shown by the tendency of the dimers to dissociate when dissolved and by the partial loss of water upon exposure to hygroscopic salts. As a result, the magnetic measurements were made on the pure crystalline solid sample, and the EPR spectra were taken as 0.1% mixtures in the nonhygroscopic, noncoordinating sodium tetraphenylborate.[12,13]

EPR. Variable-temperature EPR spectra of $Mn_2(Im)_4(OAc)_4(H_2O)$ are shown in Figure 2. The 4 K spectrum shows a series of peaks over the field range of 0−5500 G. In the temperature range 4−100 K, the signal remained unsaturated at a power of 1 mW. As the temperature was raised from 4 K, the spectral lines broadened slightly because of temperature effects, but no dramatic changes in line position or overall spectral shape occurred. J coupling of the two $S = {}^5/_2$ Mn centers yields a spin ladder with values of S ranging from 0 to 5. However, the J value of -1.29 cm^{-1} obtained from fits to magnetic susceptibility data (see below) revealed that only the $S = 1$, 2, and 3 manifolds were sufficiently populated to contribute significantly to the observed EPR spectrum at 4 K. The fact that no new peaks arose as the temperature increased and the $S = 4$ and $S = 5$ manifolds became populated suggests that temperature-dependent line broadening and zero-field splitting made the signals from these manifolds too broad to contribute to the overall spectral pattern. The integrals of the EPR spectra over this temperature range deviated from Curie behavior, as the higher energy levels became depopulated as the temperature decreased.

Because of the complexity of the EPR signals, and the fact that the contributions of the various spin manifolds to the overall EPR spectrum could not be resolved directly using variable-temperature spectra, spectral simulation was limited to the 4 K measurement, in which the $S = 4$ and $S = 5$ manifolds were not appreciably populated. The simulation utilized the spin

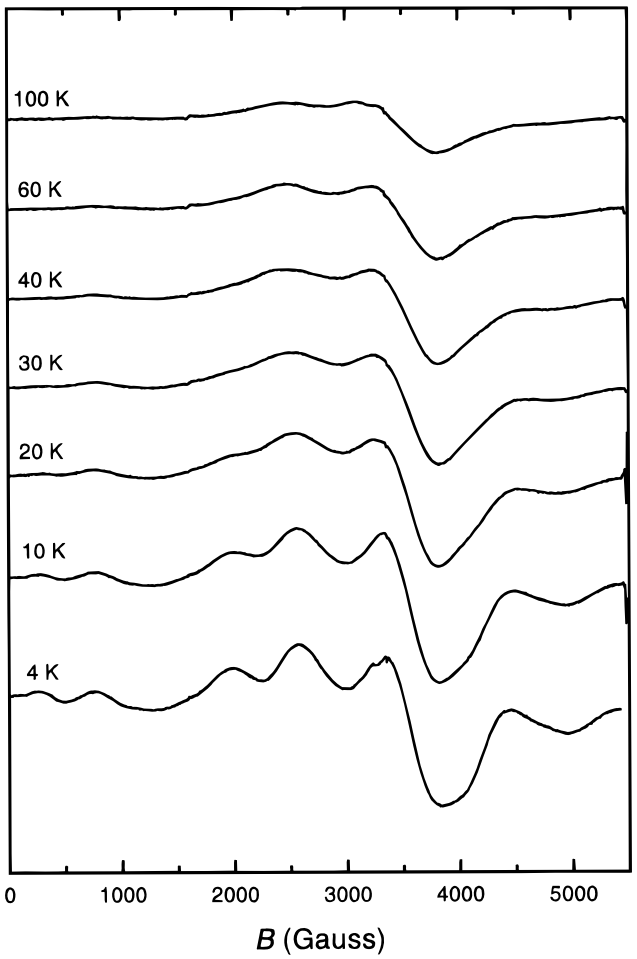

Figure 2. Variable-temperature X-band EPR spectra of $Mn_2(Im)_4(OAc)_4(H_2O)$ (0.1% in $NaBPh_4$). Conditions: 9.226 GHz microwave frequency, 1 mW microwave power, 100 kHz modulation frequency, 10 G modulation amplitude, 16.7 G/s scan rate, and 0.128 s time constant.

Hamiltonian shown in eq 1.[14] As no hyperfine splitting was

$$\hat{H} = \sum_{i=1}^{2} \beta \mathbf{B}_i \cdot \mathbf{g}_i \cdot \mathbf{S}_i + \sum_{i=1}^{2} \mathbf{S}_i \cdot \mathbf{D}_i \cdot \mathbf{S}_i - 2J\mathbf{S}_1 \cdot \mathbf{S}_2 \qquad (1)$$

observed at any temperature, the term $\sum_{i=1}^{2}\sum_{j=1}^{2} \mathbf{S}_i \cdot \mathbf{A}_{ij} \cdot \mathbf{I}_j$ was not included explicitly in the calculations. Given the high symmetry of the ^{6}A state of Mn, the contribution of spin−orbit coupling to the **g** tensor was assumed to be isotropic. In the case of strong J-coupling between two spins A and B, each resulting spin manifold can be described by the Hamiltonian in eq 2. The tensor $\boldsymbol{D}_S$ is related to the component tensors $\boldsymbol{D}_A$

$$\hat{H}_S = \beta \mathbf{B} \cdot \mathbf{g}_S \cdot \mathbf{S} + \mathbf{S} \cdot \mathbf{D}_S \cdot \mathbf{S} \qquad (2)$$

and $\boldsymbol{D}_B$ by the relation $\boldsymbol{D}_S = d_A\boldsymbol{D}_A + d_B\boldsymbol{D}_B + d_{AB}\boldsymbol{D}_{AB}$, where $\boldsymbol{D}_{AB}$ represents the anisotropic intermetal spin−spin interaction. The coefficients d_A, d_B, and d_{AB} for various spin systems have been calculated and tabulated elsewhere.[15] For $S = {}^5/_2$, $S = {}^5/_2$ systems, these coefficients for the spin-coupled system are as follows: ($S = 1$) $d_A = d_B = -16/5$, $d_{AB} = 37/10$; ($S = 2$) $d_A = d_B = -10/21$, $d_{AB} = 41/42$; ($S = 3$) $d_A = d_B = -1/45$, d_{AB}

(12) That the dimer remains intact in the sodium tetraphenylborate mixture is shown by the following observations: The χ vs T plots for the compounds in $NaBPh_4$ are identical to those for the crystalline solid except for the lower concentration. In addition, monomeric impurity gives rise to a sharp increase in χ as the temperature approaches 1.8 K, the lowest temperature in these studies; this feature is not observed. Furthermore, inclusion of a term for monomeric impurity in the magnetic susceptibility does not improve the fit. Finally, the monomeric manganese species observed upon complex dissociation give rise to a distinctive six-line EPR spectrum with hyperfine splitting of ~95 G. This signature is also not observed in $NaBPh_4$.

(13) Dilution of the sample by a further factor of 10 does not change the EPR spectrum. Hence, the sample was determined to be as magnetically dilute as can be achieved through mechanical mixing.

(14) With the exception of eq 1, individual ions are denoted by alphabetic subscripts. The term D_S and numerical subscripts are used to refer to spin manifolds in the coupled systems.

(15) Bencini, A.; Gatteschi, D. *EPR of Exchange Coupled Systems*; Springer-Verlag: Berlin, 1990.

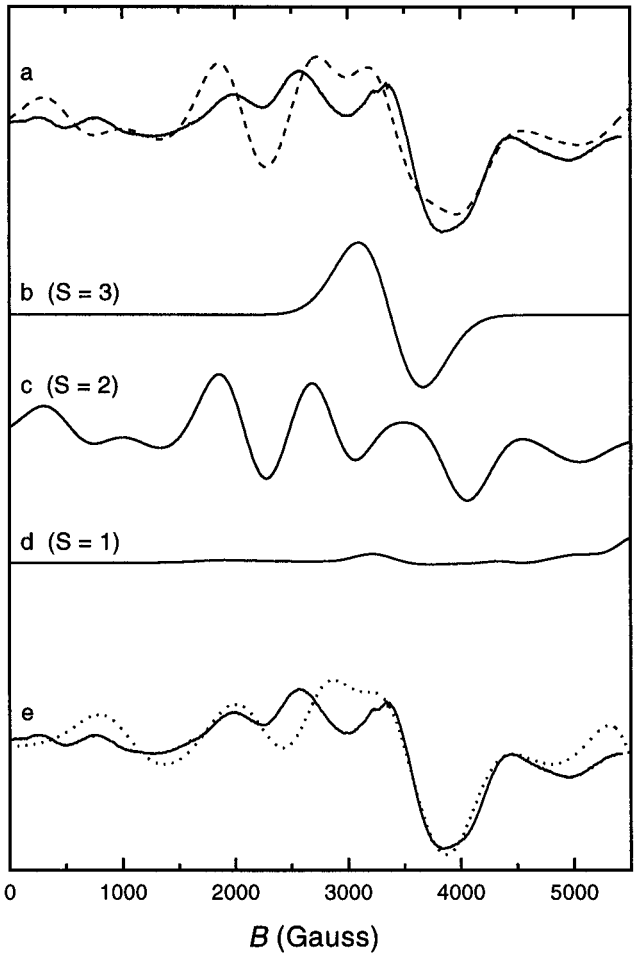

Figure 3. (a) EPR spectrum of $Mn_2(Im)_4(OAc)_4(H_2O)$ at 4 K (solid line) and simulated spectrum (dashed line). Simulation parameters: $g = 1.95$, $D = 0.095$ cm^{-1}, $E = 0$, $J = -1.29$ cm^{-1}, and line width 550 ($S = 3$), 450 ($S = 2$), and 350 G ($S = 1$). (b−d) Contributions from the $S = 3$, $S = 2$, and $S = 1$ spin manifolds to the overall spectral simulation in (a). (e) EPR spectrum of $Mn_2(Im)_4(OAc)_4(H_2O)$ at 4 K (solid line) and simulated spectrum (dotted line). Simulation parameters: $g = 1.93$, $D = 0.081$ cm^{-1}, $E = 0$, $J = -1.28$ cm^{-1}, and line width 550 ($S = 3$), 450 ($S = 2$), and 350 G ($S = 1$).

$= 47/90$; ($S = 4$) $d_A = d_B = 1/7$, $d_{AB} = 5/14$; ($S = 5$) $d_A = d_B = 2/9$, $d_{AB} = 5/18$. For $Mn_2(Im)_4(OAc)_4(H_2O)$, the observed EPR spectrum showed only one spin manifold ($S = 2$) for which an accurate value of $\boldsymbol{D}_S$ can be obtained. As a result, it was not possible to extract the relative contributions of individual ion zero-field splitting and intermetal spin−spin interactions. As both interactions are treated identically in a mathematical sense for a given spin manifold, the spectrum was simulated by attributing all of the zero-field splitting to the individual ion terms. In no way is this meant to imply that there was no intermetal spin−spin interaction; rather, it does not matter from where the effect arose for the purposes of simulation. The D value extracted from the simulation was thus an effective value, not an exact measure of either single-ion zero-field splitting or intermetal spin−spin interaction. For each spin manifold, the C_2 axis of the dimer defines one principal axis. The other two axes are determined by the relative contributions of d_A, d_B, and d_{AB}. Because of the symmetry of the system, the principal axes for each spin manifold must be coincident, such that no angular information is needed in the spectral simulation, and with a suitable choice of coordinate system, all $\boldsymbol{D}$ tensors are diagonal. This allows D to be treated as a scalar quantity. The fit for the Mn dimer thus utilized as independent parameters an isotropic g, an isotropic J, a scalar D value (identical for both ions), and

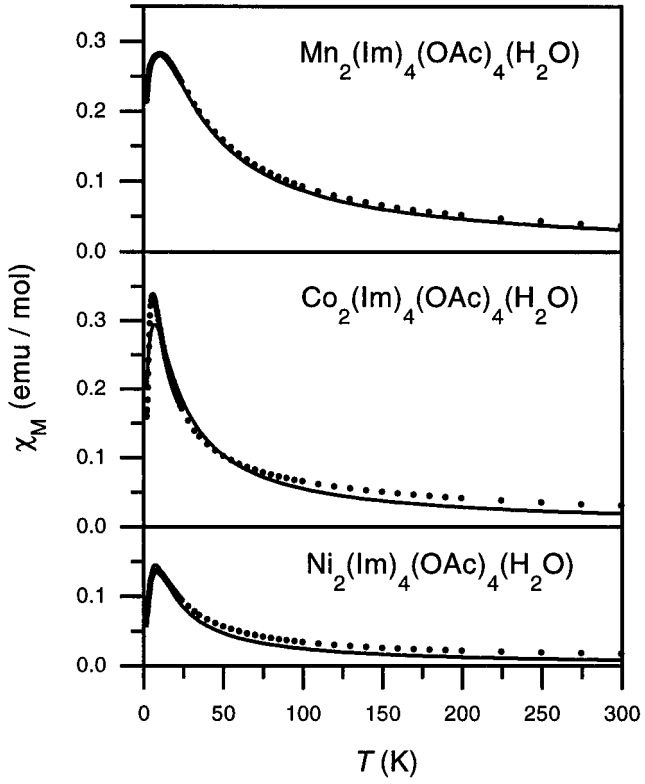

Figure 4. Magnetic susceptibility data for $Mn_2(Im)_4(OAc)_4(H_2O)$, $Co_2(Im)_4(OAc)_4(H_2O)$, and $Ni_2(Im)_4(OAc)_4(H_2O)$, over the temperature range 1.8−300 K, with fits to the data (solid lines). See text for details.

Gaussian line width parameters which encompass hyperfine coupling, D-strain, and contributions from E. Energy levels were determined by diagonalizing the 36×36 spin Hamiltonian matrix arising from the application of eq 1 to the $S = {}^5/_2$, $S = {}^5/_2$ system. The J value utilized in the simulation was determined from magnetization data (see below). D values were varied between -0.2 and 0.2 cm^{-1}. Transition probabilities were calculated explicitly using eq 3, where I is the observed

$$I \propto \langle \phi_f | \boldsymbol{\mu} \cdot \mathbf{B}_1 | \phi_i \rangle^2 \qquad (3)$$

line intensity, ϕ_i and ϕ_f are the initial and final eigenstates of the spin system, μ is the dipole moment operator, and B_1 is the excitation field. For the $S = 1$ and $S = 2$ manifolds, transition probabilities were calculated for all possible transitions within the manifold to detect the presence of any spin-forbidden transitions; for the $S = 3$, 4, and 5 manifolds, only the $\Delta M_S = 1$ transitions were analyzed. The powder pattern was generated by sampling points in a spiral pattern along the unit sphere.[16] The contributions from the $S = 1$, 2, and 3 manifolds were weighted by Boltzmann factors to yield the final spectral simulation at 4 K.

Figure 3 shows the 4 K EPR spectrum of the manganese dimer, along with the simulated fit (trace a) and the individual simulations of the $S = 1$, 2, and 3 manifolds (b−d). The simulation parameters were as follows: $g = 1.95$, $D = 0.095$ cm^{-1}, $J = -1.29$ cm^{-1}, line width 350 G ($S = 1$), 450 G ($S = 2$), 550 G ($S = 3$). Because of the large zero-field splitting in the $S = 1$ state, the resulting component spectrum was broad and did not contribute significantly to the overall spectral shape. The $S = 2$ manifold dominated the low-temperature spectrum, displaying six peaks spanning the entire spectral range. The $S = 3$ manifold gave rise to a single peak, centered at ∼3500 G,

(16) Mombourquette, M. J.; Weil, J. A. *J. Magn. Reson.* **1992**, *99*, 37−44.

as the zero-field splitting for that manifold was close to zero. Trace e in Figure 3 shows an alternative fit to the experimental spectrum, with $g = 1.93$, $J = -1.28$ cm^{-1}, and $D = 0.081$ cm^{-1}. This simulation accounts for all but one of the observed peaks and matches several of the peak positions in the experimental spectrum well.

Both the cobalt and the nickel dimers were EPR-silent over the temperature range 4−100 K. All of the spin manifolds for these dimers will be populated at these temperatures; therefore, the EPR silence is likely due to strong zero-field splitting.

Magnetism. Figure 4 shows plots of χ vs T for the manganese, cobalt, and nickel dimers at a field strength of 10 000 G, along with fits to the data. The susceptibilities were not subjected to a diamagnetic correction. All three complexes displayed antiferromagnetic behavior, with maxima in the χ vs T plots at 10.5, 6.0, and 8.0 K, respectively. The standard expression for the magnetic susceptibility of a J-coupled dimer, shown in eq 4, was inadequate for properly fitting the data, as

$$\chi = \frac{N\beta^2 g^2}{3kT} \frac{\sum_{S=0}^{S_1+S_2} S(S+1)(2S+1)\exp\left(\frac{-E_S}{kT}\right)}{\sum_{S=0}^{S_1+S_2} (2S+1)\exp\left(\frac{-E_S}{kT}\right)} \quad (4)$$

$$M = -N\frac{\sum_i \frac{\partial E_i}{\partial B}\exp(-E_i/kT)}{\sum_i \exp(-E_i/kT)} \quad (5)$$

the J-coupling was found to be quite weak. The more general expression given in eq 5 was used for all magnetization fits. The energies E and the magnetic moments $\partial E/\partial B$ were calculated using spin Hamiltonian matrix diagonalization. Energy levels were calculated with the magnetic field aligned along the principal molecular axes, and the M and χ values were calculated using eq 5. Nuclear hyperfine terms were ignored in these calculations. The average of the χ values, $\chi_{av} = (\chi_x + \chi_y + \chi_z)/3$, was used to fit the experimental data. The parameters g and J were optimized through simplex fitting,[17] utilizing the EPR-NMR program and a program custom-written in our laboratory. Several random initial guesses of g and J were made, and the fitting routine varied the two parameters so as to minimize the quantity $\sum(\chi_{measd} - \chi_{calcd})^2$. The fits were weighted toward the low-temperature data by virtue of the larger number of data points taken in that range.

Values of g and J for the metal dimers, as determined from simplex fitting, were as follows: $g = 1.89$, $J = -1.29$ cm^{-1} for $Mn_2(Im)_4(OAc)_4(H_2O)$; $g = 2.22$, $J = -1.60$ cm^{-1} for $Co_2(Im)_4(OAc)_4(H_2O)$; and $g = 2.04$, $J = -2.47$ cm^{-1} for $Ni_2(Im)_4(OAc)_4(H_2O)$. For the manganese dimer, a D value of 1020 G, derived from the EPR data, was included in the fitting. The reduced g value for the Mn dimer as compared with the EPR simulation most likely arose from errors in sample weight, as the g value obtained from susceptibility measurements is highly sensitive to this quantity and is thus not very accurate. For the cobalt and nickel dimers, D was not included in the magnetic susceptibility analysis, as there was no independent means of measuring this quantity. The EPR silence of the cobalt and nickel dimers at X-band suggested that the value of D is non-negligible; however, simulations of the magnetic susceptibility of the two dimers suggested that the error introduced in J by ignoring D is only on the order of a few tenths of a wavenumber. Including D and temperature-independent magnetism as variables improved the fit to the magnetic susceptibility data for the nickel and cobalt dimers, but the large number of variables cast doubt on the reliability of the numbers obtained.

Discussion

Transition metal complexes containing the μ-aquo−bis(μ-carboxylato) ligand environment have been known for over two decades. Interest in these compounds as models for enzyme active sites was spurred by the crystal structure determination of hemerythrin,[18] which contains the μ-oxo−bis(μ-carboxylato) unit, as well as by later structure determinations of the related diiron proteins ribonucleotide reductase[19] and methane monooxygenase.[20] Structure determinations of hydrolases and other binuclear metalloenzymes have revealed a large diversity of active site structures. In order to achieve an understanding of such active site structures through spectroscopic probes, and to learn the relationships between electronic structure and reactivity in these proteins, detailed study of model systems is necessary. Complexes with the μ-aquo−bis(μ-carboxylato) structure have been difficult to study in this regard for two main reasons. First, J-coupling in these complexes gives rise to spin manifolds with integer spins, such that Kramer's doublets do not exist, and significant zero-field splitting can render the compounds EPR-silent. Second, J-coupling in complexes with a μ-aquo bridge is generally very small, being of the same order of magnitude as the Zeeman splitting and zero-field splitting of the component metals, so that appreciable mixing can occur between the various spin manifolds. Hence, perturbation theory is often ineffective in dealing with these systems. With regard to the former point, manganese(II), which possesses a symmetric ^{6}A ground electronic state, often has a zero-field splitting small enough to allow detection of its dimers by EPR techniques. Manganese(II) dimers have been studied effectively by EPR in single crystals of manganese-doped solid state materials;[21−24] however, for discrete molecules, which are normally analyzed as randomly oriented solids or frozen solutions, analysis is complicated by orientation effects and by the large number of energy levels involved. Several analyses of binuclear manganese(II) complexes have been performed,[25−31] utilizing the temperature dependence of specific EPR transitions, spectral deconvolution techniques or simulation by second-order perturbation theory.

(17) Press, W. H.; Flannery, B. P.; Teukolsky, S. A.; Vetterling, W. T. *Numerical Recipes in C: The Art of Scientific Computing*; Cambridge University: Cambridge, U.K., 1988.

(18) Holmes, M. A.; Stenkamp, R. E. *J. Mol. Biol.* **1991**, *220*, 323−337.
(19) Nordlund, P.; Eklund, H. *J. Mol. Biol.* **1993**, *232*, 123−164.
(20) Rosenzweig, A. C.; Frederick, C. A.; Lippard, S. J.; Nordlund, P. *Nature* **1993**, *366*, 537−543.
(21) Coles, B. A.; Orton, J. W.; Owen, J. *Phys. Rev. Lett.* **1960**, *4*, 116−117.
(22) Harris, E. A.; Owen, J. *Phys. Rev. Lett.* **1963**, *11*, 9−10.
(23) Harris, E. A. *J. Phys. C: Solid State Phys.* **1972**, *5*, 338−352.
(24) McPherson, G. L.; Chang, J. R. *Inorg. Chem.* **1976**, *15*, 1018−1022.
(25) Laskowski, E. J.; Hendrickson, D. N. *Inorg. Chem.* **1978**, *17*, 457−470.
(26) Mathur, P.; Dismukes, G. C. *J. Am. Chem. Soc.* **1983**, *105*, 7093−7098.
(27) Mabad, B.; Cassoux, P.; Tuchagues, J.-P.; Hendrickson, D. N. *Inorg. Chem.* **1986**, *25*, 1420−1431.
(28) Kessissoglou, D. P.; Butler, W. M.; Pecoraro, V. L. *Inorg. Chem.* **1987**, *26*, 495−503.
(29) Flassbeck, C.; Wieghardt, K.; Bill, E.; Butzlaff, C.; Trautwein, A. X.; Nuber, B.; Weiss, J. *Inorg. Chem.* **1992**, *31*, 21−26.
(30) Pessiki, P. J.; Khangulov, S. V.; Ho, D. M.; Dismukes, G. C. *J. Am. Chem. Soc.* **1994**, *116*, 891−897.
(31) Khangulov, S. V.; Pessiki, P. J.; Barynin, V. V.; Ash, D. E.; Dismukes, G. C. *Biochemistry* **1995**, *34*, 2015−2025.

In addition, EPR measurements have been made on native dimanganese enzymes and Mn-reconstituted binuclear sites in other proteins.[31−37] However, despite the presence of three structurally characterized manganese dimers with the $Mn_2(\mu\text{-}H_2O)(\mu\text{-}OAc)_2$ core, no EPR spectrum of such a species has been reported to date.

The complex $Mn_2(Im)_4(OAc)_4(H_2O)$ is a reasonably simple system for observing the electronic structure of Mn^{II}/Mn^{II} dimers. The complex possesses a C_2 axis relating the two metal centers and lacks discernable hyperfine coupling, allowing a simulation requiring a relatively small set of independent parameters. Furthermore, since the $S = 4$ and $S = 5$ spin manifolds are not appreciably populated at 4 K, the simulation problem acquires further simplicity. The parameters g, D, J, and three line width values were sufficient to reproduce the major spectral features of the observed EPR spectrum, specifically the number and approximate location of the seven discernable peaks in the spectrum and, to a reasonable extent, line intensities. As the spectrum arising from the $S = 1$ manifold is rather featureless, the line width for this manifold has little effect on the overall spectrum. The line widths for the $S = 2$ and $S = 3$ spectra, while having been chosen on the basis of their ability to fit the observed spectrum, also reflect the known trend of increasing line widths with increasing S. It is worth noting that a recent simulation of the fluoride-inhibited Mn−catalase from *Lactobacillus plantarum*[37] shows a spectral pattern similar to that observed for $Mn_2(Im)_4(OAc)_4(H_2O)$; however, the pattern for Mn−catalase arises from a larger J value and smaller D_S values, making the resemblance of the two simulations fortuitous.

The lack of complete agreement between the experimental and simulated spectra for $Mn_2(Im)_4(OAc)_4(H_2O)$ with regard to line positions is not surprising, given the small number of parameters utilized. As is shown by the alternative fit to the EPR spectrum, where $D = 0.081$ cm^{-1} instead of 0.095 cm^{-1}, there remains a small range over which the parameters can be varied while still yielding an acceptable fit to the observed spectrum. To the extent that the Hamiltonian correctly describes the spin system of the dimer, the matrix diagonalization techniques utilized in the simulation should faithfully reproduce the EPR spectrum. Hence, further improvements in the fit will likely require the use of additional terms in the Hamiltonian and perhaps a more sophisticated treatment of line widths.

Two electronic parameters used widely for relating spectroscopic and structural data are the Heisenberg exchange J and the zero-field splitting parameter D. J is a measure of orbital overlap and thus depends on metal−metal separation, the identity of bridging ligands which mediate the superexchange, and the M−L−M angle, where L is the bridging ligand. For spin-coupled dimers, D_S for a given spin manifold is composed of contributions from the single ion ZFS and from the intermetal spin−spin interaction and, thus, is a measure of both the anisotropy in the crystal field of the individual metals, and the internuclear separation, as the spin−spin interaction has a $1/r^3$ distance dependence.

Khangulov and co-workers have found an empirical linear relationship in proteins and synthetic inorganic complexes between $Mn^{II}-Mn^{II}$ distances determined by X-ray crystallography and D_2, the zero-field splitting of the quintet ($S = 2$) state of the dimer.[31] The compounds utilized in generating this relationship span a range in Mn−Mn distances of 3.06−3.66 Å and a range of D_2 of −0.182 to −0.034 cm^{-1}. This relationship is explained as the result of two opposing effects: the $1/r^3$ dependence of the intermetal spin−spin interaction and a decrease in the single-ion ZFS (D_C) as the metal−metal distance decreases and the bridging ligands become less ionic in character. As the principal contribution to the 4 K spectrum of $Mn_2(Im)_4(OAc)_4(H_2O)$ is the $S = 2$ manifold, the value of D_2 is readily obtained for this complex. Given the observed Mn−Mn distance of 3.777 Å, one would expect a D_2 value very close to zero. However, the observed D_2 value of −0.090 cm^{-1} (−20/21 × 0.095) for this dimer deviates significantly from the linear relationship. There are two possible reasons for this discrepancy. First, the relationships between metal−metal separation and both D_C and the spin−spin interaction are inherently nonlinear, so that even if a linear relationship between metal−metal distance and D_2 exists over a given range of M−M distances, the linear relationship is likely to break down at very long or very short distances. Second, D_C and the spin−spin interaction are in general independent parameters. If the terminal ligands on the metal centers provide the major asymmetry in the crystal field, rather than the bridging ligands, then the metal−metal separation is expected to have very little effect on D_C. Hence, a certain amount of caution is necessary in inferring metal−metal distances from the single parameter D_2.

In the interpretation of J values, the identity of the bridging ligands generally is the most prominent factor. While bridging ligands control metal−metal separations, their principal role in mediating exchange coupling lies in their ability to provide orbital overlap through the ligand orbitals. Table 1 shows the magnetic parameters for the Mn, Co, and Ni dimers, along with values for selected analogous compounds in the literature.[38−50] For those compounds for which no J value is reported, the Néel temperature is given instead. The values of T_N for the cobalt and nickel dimers in this work are included for comparison. More complete tabulations of structural and magnetic data for biomimetic, binuclear manganese and nickel complexes have been published.[31,51] In addition, other dicobalt and dinickel compounds containing the μ-aquo−bis(μ-carboxylato) motif

(32) Reczkowski, R. S.; Ash, D. E. *J. Am. Chem. Soc.* **1992**, *114*, 10992−10994.
(33) Antaniaitis, B. C.; Brown, R. D., III; Chasteen, N. D.; Freedman, J. H.; Koenig, S. H.; Lilienthal, H. R.; Peisach, J.; Brewer, C. F. *Biochemistry* **1987**, *26*, 7932−7937.
(34) Schulz, C.; Bertini, I.; Viezzoli, M. S.; Brown, R. D., III; Koenig, S. H.; Coleman, J. E. *Inorg. Chem.* **1989**, *28*, 1490−1496.
(35) Atta, M.; Nordlund, P.; Åberg, A.; Eklund, H.; Fontecave, M. *J. Biol. Chem.* **1992**, *267*, 20682−20688.
(36) Poyner, R. R.; Reed, G. H. *Biochemistry* **1992**, *31*, 7166−7173.
(37) Meier, A. E.; Whittaker, M. M.; Whittaker, J. W. *Biochemistry* **1996**, *35*, 348−360.
(38) Caneschi, A.; Ferraro, F.; Gatteschi, D.; Melandri, M. C.; Rey, P.; Sessoli, R. *Angew. Chem., Int. Ed. Engl.* **1989**, *28*, 1365−1367.
(39) Yu, S.-B.; Lippard, S. J.; Shweky, I.; Bino, A. *Inorg. Chem.* **1992**, *31*, 3502−3504.
(40) Bossek, U.; Wieghardt, K.; Nuber, B.; Weiss, J. *Inorg. Chim. Acta* **1989**, *165*, 123−129.
(41) Wieghardt, K.; Bossek, U.; Nuber, B.; Weiss, J.; Bonvoisin, J.; Corbella, M.; Vitols, S. E.; Girerd, J. J. *J. Am. Chem. Soc.* **1988**, *110*, 7398−7411.
(42) Turpeinen, U.; Ahlgrén, M.; Hämäläinen, R. *Acta Crystallogr.* **1982**, *B38*, 1580−1583.
(43) Turpeinen, U.; Hämäläinen, R.; Reedijk, J. *Polyhedron* **1987**, *6*, 1603−1610.
(44) Turpeinen, U.; Ahlgrén, M.; Hämäläinen, R. *Finn. Chem. Lett.* **1977**, 246−251.
(45) Turpeinen, U. *Finn. Chem. Lett.* **1976**, 173−178.
(46) Turpeinen, U. *Finn. Chem. Lett.* **1977**, 36−41.
(47) Turpeinen, U. *Finn. Chem. Lett.* **1977**, 123−128.
(48) Ahlgrén, M.; Turpeinen, U.; Hämäläinen, R. *Acta Chem. Scand.* **1978**, *A32*, 189−194.
(49) Chaudhuri, P.; Küppers, H.-J.; Wieghardt, K.; Gehring, S.; Haase, W.; Nuber, B.; Weiss, J. *J. Chem. Soc., Dalton Trans.* **1988**, 1367−1370.
(50) Wages, H. E.; Taft, K. L.; Lippard, S. J. *Inorg. Chem.* **1993**, *32*, 4985−4987.
(51) Halcrow, M. A.; Christou, G. *Chem. Rev.* **1994**, *94*, 2421−2481.

Table 1. Metrical and Magnetic Data for Selected Dimeric Divalent Metal Complexes

compound[a]	M−M (Å)	M−O−M[b] (deg)	J[c] (cm^{-1})	ref
$Mn_2(H_2O)(Im)_4(OAc)_4$	3.777	114.4	−1.29	11, this work
$Mn_2(H_2O)_3(F_5C_2COO)_4L_2$	3.739	114.6	−1.65	38
$Mn_2(H_2O)(piv)_4(Me_2bpy)_2$	3.5950	110.2	−2.73	39
$Mn_2(H_2O)(OAc)_4(tmeda)_2$	3.621	110.0	−2.952	39
$[Mn_2(OH)(OAc)_2(tmeda)_2]^+$	3.351	109.4	−9	40
$[Mn_2(OAc)_3(Me_3tacn)]^+$	4.034	−	−1.7	41
$Co_2(H_2O)(Im)_4(OAc)_4$	3.687	117.2	−1.60 (T_N = 6.0)	11, this work
$Co_2(H_2O)(OAc)_4(tmeda)_2$	3.597	115.1	T_N = 3.0	42, 43
$Co_2(H_2O)(ClCH_2COO)_4(tmeda)_2$	3.621	113.5	T_N = 4.8	42, 43
$Co_2(H_2O)(Cl_3CCOO)_4(tmeda)_2$	3.696	116.1	T_N = 4.3	43
$Ni_2(H_2O)(Im)_4(OAc)_4$	3.635	119.0	−2.47 (T_N = 8.0)	11, this work
$Ni_2(H_2O)(OAc)_4(tmeda)_2$	3.563	117.2	T_N < 2	43, 44
$Ni_2(H_2O)(ClCH_2COO)_4(tmeda)_2$	3.567	117.4	T_N = 3.0	43, 45−47
$Ni_2(H_2O)(Cl_2CHCOO)_4(tmeda)_2$	3.657	118.1	T_N = 4.0	43, 48
$[Ni_2(OH)(OAc)_2(Me_3tacn)_2]^+$	3.400	115.2	−4.5	49
$[Ni_2(OAc)_3(urea)(tmeda)_2]^+$	3.4749	109.8[d]	−0.9	50

[a] Abbreviations: Im = imidazole; L = 2-ethyl-4,4,5,5-tetramethyl-3-oxo-4,5-dihydro-1*H*-imidazolyl-1-oxyl; Me_3tacn = *N*,*N*′,*N*″-1,4,7-triazacyclononane; OAc = acetate; piv = pivalate; py = pyridine; tmeda = *N*,*N*,*N*′,*N*′-tetramethylethylenediamine. [b] Angle formed by bridging aquo, hydroxo, or monodentate acetato group. [c] $H = -2JS_1S_2$. [d] One of the acetate ligands bridges the two Ni centers through a single oxygen atom.

have been crystallographically characterized but have not been subjected to detailed magnetic study.[52−59]

It is well-known that, for coupled metal centers with bridging oxygen-containing ligands, the strength of the coupling varies according to the trend $H_2O < OH^- < O^{2-}$. The compounds listed in Table 1 demonstrate this trend. For the μ-aquo dimers in Table 1, $|J| < 3\ cm^{-1}$, a value indistinguishable from those arising from species containing only carboxylate bridges. Hence, the presence of a bridging water molecule at an enzyme active site cannot be demonstrated by magnetic susceptibility alone.

In that both bridging and terminal aquo groups have been observed in hydrolase crystal structures and model compounds, the mode of water activation during turnover of these enzymes must be addressed. Studies of phosphate ester hydrolysis by transition metal complexes suggest that the principal contributions of the metal in catalyzing the reaction are in bringing the substrates into close proximity, and in decreasing the pK_a of a bound water molecule, to generate a more nucleophilic hydroxyl group.[60] The presence of a binuclear site in the hydrolase enzymes suggests that perhaps one metal ion is involved in the activation of substrate, while the second one activates water. However, because the known active site structures can in principle accommodate alternative binding modes for substrate and water, the orientation of the reactants during the course of the hydrolysis reaction may not be the same for all hydrolases. It is likely that mechanistic details will differ somewhat with the identity of the metals in the enzyme active site. Further understanding of the hydrolysis reaction will of necessity rely on the use of biomimetic complexes, especially those that more faithfully duplicate the active site structure of the known hydrolase enzymes.

Conclusion

As the first μ-aquo manganese(II) dimer characterized by EPR, the complex $Mn_2(Im)_4(OAc)_4(H_2O)$ provides a guideline for the interpretation of enzyme EPR spectra. The symmetry of the molecule results in a relatively simple spectrum, which has been successfully simulated through the use of matrix diagonalization techniques. The principal contribution to the spectrum is the $S = 2$ manifold, with lesser contributions from the $S = 1$ and $S = 3$ manifolds. Parallel study of the magnetic susceptibilities of the manganese, cobalt, and nickel dimers reveals small antiferromagnetic J coupling for all of the complexes, underscoring the difficulty of using magnetic susceptibility data to infer structural information. Nevertheless, the presence of a series of isostructural bimetallic complexes containing a range of transition metals and a μ-aquo group will allow a study of the effect of the transition metal on both spectroscopic and reactivity properties related to the ability of enzymes to catalyze the hydrolysis reaction.

Acknowledgment. Funding for this work was provided by NIH Grant GM22432 from the National Institute of General Medical Sciences, U.S. Public Health Services. X.-y.L. acknowledges the support of this project by RGC-CERG and HKUST. B.E.S. is the recipient of a National Science Foundation Postdoctoral Fellowship. We thank Jeff Clites for experimental assistance.

IC960988R

(52) Ahlgrén, M.; Hämäläinen, R.; Turpeinen, U. *Finn. Chem. Lett.* **1983**, 125−128.
(53) Hagen, K. S.; Lachicotte, R.; Kitaygorodsky, A.; Elbouadili, A. *Angew. Chem., Int. Ed. Engl.* **1993**, *32*, 1321−1324.
(54) Lachicotte, R.; Kitaygorodskiy, A.; Hagen, K. S. *J. Am. Chem. Soc.* **1993**, *115*, 8883−8884.
(55) Hagen, K. S.; Lachicotte, R.; Kitaygorodskiy, A. *J. Am. Chem. Soc.* **1993**, *115*, 12617−12618.
(56) Gulya, A. P.; Shova, S. G.; Novitskii, G. V.; Mazus, M. D. *Russ. J. Coord. Chem.* **1994**, *20*, 105−115.
(57) Ahlgrén, M.; Hämäläinen, R.; Turpeinen, U. *Cryst. Struct. Commun.* **1977**, *6*, 829−834.
(58) Ahlgrén, M.; Turpeinen, U. *Acta Crystallogr.* **1982**, *B38*, 276−279.
(59) Kennard, C. H. L.; O'Reilly, E. J.; Smith, G. *Polyhedron* **1984**, *3*, 689−693.
(60) Hendry, P.; Sargeson, A. M. *Prog. Inorg. Chem.* **1990**, *38*, 201−258.